Optik - International Journal for Light and Electron Optics 279 (2023) 170746

Contents lists available at ScienceDirect

Optik - International Journal for Light and Electron Optics

journal homepage: www.elsevier.com/locate/ijleo

Original research article

Geometric optical transfer function and pupil sampling patterns

José A. Díaz [a,*], Rafael Navarro [b]

[a] Departamento de Óptica. Universidad de Granada, 18071, Granada, Spain
[b] INMA, Consejo Superior de Investigaciones Científicas and Universidad de Zaragoza, 50009 Zaragoza, Spain

ARTICLE INFO

Keywords:
Imaging systems
Optical transfer functions
Optical aberrations
Optical raytracing

ABSTRACT

We have studied several pupil sampling patterns for calculating the optical transfer function corresponding to actual non-diffraction limited optical imaging systems, in the low range of spatial frequencies, i.e., where the geometric approach is valid, by means of the Fourier Transform of the spot diagram. Then, we have compared the diffraction and the geometric optical transfer functions to ascertain if there is a sampling pattern that accurately calculates the latter within a 5% of difference, and having less number of sampling points. The results show that, overall, the non redundant spiral pupil sampling provides the best choice. This could be valuable when optimizing or characterizing optical imaging systems in the non-diffraction limited range by harnessing raytracing.

1. Introduction

The imaging optical systems design relies on commercial or proprietary software that essentially trace finite rays from the object point through the pupil of the system, to the image plane [1–4]. Then, complex and more advanced analysis can be done including optimization, and tolerancing methods [5–8]. Although there are also open source libraries implemented in programming languages such as Python [9–13], these currently cannot compete with professional software. These libraries are mainly used in academic, or non professional environments.

From raytracing data, multiple analysis can be performed to evaluate the image quality, ranging from the geometrical optics approximation to wave diffraction theory. However, image quality ultimately should be based on measurable characteristics of the image obtained. In this sense, the modulation transfer function (MTF) is proven to be the most valuable way to characterize the performance of an imaging optical system over the field of view (FOV). This function is the modulus of the optical transfer function (OTF), and provides the contrast in the image related to that in the object, as a function of the spatial frequency resolved by the imaging system [14,15]. The MTF accounts for the effects of both aberrations and diffraction in the wavefront at the system exit pupil. When aberrations are large, i.e., the relative effect of diffraction is small, then the geometrical optics can be a fair enough approximation.

Several authors did the pioneering work on the numerical calculation of both the diffraction optical transfer function (DOTF), and the geometrical transfer function (GOTF) [16–19]. It is well known that the GOTF approximates the DOTF only for large aberrations [20–22]. In a recent paper, the geometrical, and diffraction imaging in the space and frequency domains were compared [23]. The threshold values of primary aberrations studied, for which the two OTFs differ by no more than 5% or 10% over a frequency range of interest where the DOTF falls from a maximum value of 1 to a value of 0.1 were given. The results reported confirm that the amount of optical aberrations for which the GOTF approximates well the DOTF were about 2λ, and higher.

* Corresponding author.
E-mail address: jadiaz@ugr.es (J.A. Díaz).
URL: https://www.researchgate.net/profile/Jose_Diaz71 (J.A. Díaz).

https://doi.org/10.1016/j.ijleo.2023.170746
Received 26 October 2022; Received in revised form 17 February 2023; Accepted 3 March 2023
Available online 8 March 2023

An alternative numerical approach to the calculation of the GOTF is based on the Fourier transform (FT) of the spot diagram data [23,24]. One can expect that the higher is the number of ray traced, the more dense is the spot diagram, and, thus, the more accurate will be the GOTF calculation. However, it has been proven that this is not necessarily true, that is, a dense sampling in the pupil for tracing rays is not needed to obtain a valid GOTF approximation to the DOTF [25].

Further, it follows that this can be a trade-off when looking for an advantage for repetitive OTF calculations when optimizing a design of an optical imaging system with large aberrations at various optical wavelengths, and field angles. It has been put forward the fact that the calculation of the DOTF is faster than that of the GOTF, considering a similar number of pupil sampling points of the imaging system, which follows a rectangular pattern [25].

However, the GOTF calculation could be improved by considering several pupil sampling patterns having different number of points, and similar level of DOTF approximation accuracy. That number for some of the patterns even may be quite lower compared to the that required to calculate the DOTF by the Fast Fourier Transform (FFT) of the incoherent point spread function (PSF), or by discrete autocorrelation (DA) of the pupil function.

In this paper, we examine and compare the number of sampling points required for each pupil pattern to calculate the corresponding GOTF from FT of the spot diagram data, of three actual optical imaging systems. These systems are non-diffraction limited and have different optical imaging quality for on- as well for off-axis due to their aberration combinations, which would enable to extract general conclusions from the results of the study. The calculated GOTF, and the DOTF should differ by no more than 5%. Some of the pupil patterns are those commonly used for obtaining an spot diagram, such as the rectangular, the hexapolar, and the uniform random pattern [5,6,8]. In addition, we have included three more of them: the non uniform polar, the spiral, and the Bos pattern, the last two having demonstrated to be useful when improving the reconstruction of the wavefront aberration in terms of the Zernike circular polynomial basis [15,26] from transverse ray aberration data gathered by means of raytracing [27–30].

2. Theory

Consider an imaging system having a circular pupil with an aberration function $W(x, y)$ in units of wavelength λ, where (x, y) are the coordinates of a pupil point normalized by the radius a of its pupil. Given that the pupil function for a uniformly but aberrated pupil is:

$$P(x, y) = \exp[2\pi i W(x, y)] \tag{1}$$

then, the incoherent PSF of the system at a point (x_i, y_i) normalized by λF (F being the focal ratio of the image-forming light cone) is given by [14,15]

$$PSF\left(x_i, y_i\right) = \frac{1}{\pi^2}\left|\iint_{\mathcal{A}} P(x, y)\exp\left[-\pi i\left(x_i x + y_i y\right)\right]\mathrm{d}x\mathrm{d}y\right|^2, \tag{2}$$

where $\mathcal{A}$ is the unit circle.

Its corresponding incoherent optical transfer function, the DOTF, $\tau(\xi, \eta)$, is given by the Fourier transform of the PSF, or equivalently, by the autocorrelation of the pupil function [14–16], which can be expressed by taking into account the aberration difference function at the spatial frequency (ξ, η) in units of the diffraction cutoff frequency $1/\lambda F$, and in Cartesian coordinates, as

$$Q(x, y; \xi, \eta) = W(x + \xi, y + \eta) - W(x - \xi, y - \eta), \tag{3}$$

and hence

$$\tau(\xi, \eta) = \frac{1}{\pi}\iint_{\text{overlap area}} \exp[2\pi i Q(x, y; \xi, \eta)]\mathrm{d}x\ \mathrm{d}y \tag{4}$$

The aberrated GOTF, $\tau_g(\xi, \eta)$, corresponding to a spatial frequency (ξ, η) is given by [15,17]

$$\tau_g(\xi, \eta) = \frac{1}{\pi}\iint_{\mathcal{A}} \exp\left[2\pi i\left(\xi x_i + \eta y_i\right)\right]\mathrm{d}x\ \mathrm{d}y \tag{5}$$

where

$$\left(x_i, y_i\right) = 2\left(\frac{\partial W}{\partial x}, \frac{\partial W}{\partial y}\right) \tag{6}$$

are the transverse ray aberrations in units of λF [31,32]. Although the transverse ray aberrations can be obtained from the wave aberration function, they may be determined simply by tracing the rays up to the image plane.

The GOTF can also be calculated as the FT of the spot diagram [24,25,33]:

$$\tau_g(\xi, \eta) = \frac{1}{N}\sum_{i=1}^{N} e^{-2\pi i(\xi x_i + \eta y_i)} \tag{7}$$

where N is the number of spots obtained by tracing the same number of rays through the pupil. This expression neglects the variation in spot density that acts as an apodization of the pupil. Nevertheless, its effect on the transfer function is small compared to that of an aberration, and can be neglected.

Results reported recently [25] also indicate that the GOTF obtained from Eq. (7) is numerically the same as that obtained from Eq. (5). Thus, the spot diagram has the advantage that it avoids the singularities of the analytical geometrical PSF for certain aberrations, such as spherical aberration or coma [32].

3. Numerical methods of the OTF calculation and pupil sampling patterns

3.1. Calculation of the DOTF

We calculate the DOTF in Eq. (4) by using discrete autocorrelation (DA) of the pupil function. Thus, if the pupil function is sampled at $N \times N$ points, the DOTF is calculated at the discrete spatial frequency (ξ, η) as

$$\tau(\xi,\eta) = \frac{1}{\pi} \sum_{x=-(N-1)/2}^{(N-1)/2} \sum_{y=-(N-1)/2}^{(N-1)/2} \exp[2\pi i W(x,y)] \exp[-2\pi i W(x-\xi, y-\eta)] \tag{8}$$

In this work, the pupil function was required to be sampled at $64 \times 64\,(4096)$ points yielding 64×64 DOTF values truncated in the spatial frequency domain to guarantee accuracy in the calculation [23,25], although in some cases a sampling comprising $32 \times 32\,(1024)$ points would have been accurate enough. As the DOTF is a complex function, the modulus of the DOTF, the DMTF, $|\tau(\nu)|$, has been plotted to a spatial frequency for which its value was around 0.1.

3.2. Calculation of the GOTF

We calculate the GOTF by using Eq. (7), and considering the different pupil sampling patterns adopted to obtain its corresponding spot diagram. Similarly, as the GOTF is a complex function, the modulus of the GOTF, the GMTF, $|\tau_g(\nu)|$, has been plotted to the same spatial frequency as for the DMTF, for comparison.

3.3. Pupil sampling patterns

The spot diagram was obtained from the wavefront aberration function, $W(x, y)$, and by using Eq. (6) at the points in the pupil sampled following these patterns:

(a) Rectangular pattern (C).
This one is easy to implement in any software to show spot diagrams for imaging systems, as well as the most intuitive to trace rays in the system [1–4]. It consists in sampling the pupil by a rectangular grid being the nodes the intersection points.

(b) Non uniform polar pattern (P)
This pattern is a slightly modified version of that commonly used in commercial software, the polar one [6]. It consists in sampling the pupil by set of circles and spokes, being the nodes the intersection points. The non uniformity is done by increasing the circle radius nonlinearly (with an exponent of 1/2) from 0 to 1 to keep the sampling density approximately constant within the pupil, but more dense in its boundary.

(c) Hexapolar pattern (H)
This pattern is also another one commonly used in commercial and open source software [1,2,6,27]. It consists in sampling the pupil by a grid with node coordinates (ρ_j, θ_j), with $\rho_j = 1/n, \ldots, 1$, and $\theta_j = \pi/(3n\rho_j), \ldots, 2\pi$, where n is the number of circles.

(d) Random pattern (R)
In this pattern, the sampling consists in a set of random points uniformly distributed within the pupil [1,6,27].

(e) Spiral pattern (S)
This pattern, also called non redundant pattern [27,28], is a set of points describing an spiral which become dense as they are close to the pupil boundary. Briefly, the radial coordinate follows the relationship $\rho(\theta) = \sqrt[4]{\theta/\theta_{max}}$, where $\theta_{max} = 2\pi N_c$, being N_c the number of spiral cycles, and the number of samples per cycle related with the total number of points, I, by $\delta\theta = \theta_{max}/(I-1)$.

(f) Bos pattern (B)
This pattern is another non redundant one [29,30], and it consists in a set of points having the polar coordinates $(\rho_j, 2\pi(s_j - 1)/n_j)$, with

$$\rho_j(n) = 1.1565\zeta_{j,n} - 0.76535\zeta_{j,n}^2 + 0.60517\zeta_{j,n}^3$$

where $\zeta_{j,n}$ are zeros of the $(n+1)$-st Chebyshev polynomial of the first kind,

$$\zeta_{j,n} = \cos\left(\frac{(2j-1)\pi}{2(n+1)}\right), \quad j = 1, \ldots, \left\lfloor \frac{n}{2} \right\rfloor + 1$$

being $\lfloor \cdot \rfloor$ the floor function, $s_j = 1, \ldots, n_j$ and n the maximum Zernike radial order.

Fig. 1 shows the sampling of the pupil by using these patterns, and having about the same number of points (in parenthesis), as the generating function hinders that the set of rays will be the same for all of them.

In this work, the number of sampling points in each pattern was increased up to that for which the maximum difference between the DMTF and the GMTF calculated was less than or about 5%. In the case this could not be accomplished, then, that number was not longer increased.

All the calculations were done in a 3.4 GHz PC desktop with an Intel i7 processor having 8 cores, 16 Gb of RAM, running Windows 10 OS (64 bits), and by using Mathematica™ [34].

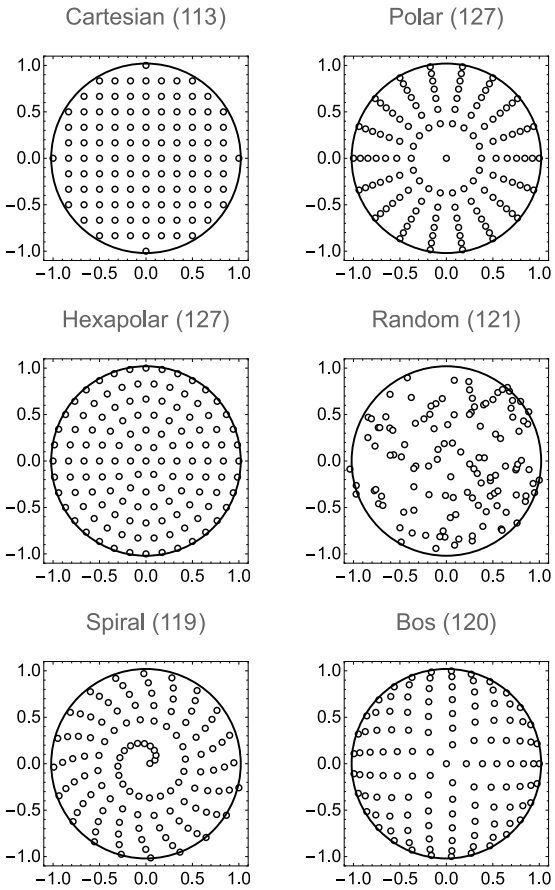

Fig. 1. Geometrical pupil sampling patterns utilized for obtaining the FT from their corresponding spot diagram. The number of sampling points is indicated in parenthesis in each case, and as an example.

4. Numerical examples

We calculate, and plot the DMTF, and the GMTF functions for three imaging systems [35]:

1. An f/2.5 double Gauss lens for use in a motion-picture camera (35-mm film).
2. An f/2.8 telephoto lens for use with a single-lens reflex (SLR) camera.
3. An f/2 projection lens for 70 mm cinematography.

All of them work at a wavelength of 546 nm, and their respective FOV are 24°, 6°, and 160°, respectively.

The wavefront aberration function, $W(x, y)$, was determined by fitting the OPD data to the first 37 orthonormal Zernike circle polynomials, for on–, as well as for off-axis field points, and for the three systems:

$$W(x, y) = \sum_{j=1}^{37} a_j Z_j(x, y) \tag{9}$$

We used ZEMAX software [1], and the obtained Zernike coefficients, a_j, are listed in Table 1 [23]. We have also checked that the wavefront at the exit pupil of the systems is basically circular in each case, thus allowing to sample the pupil accurately by using each pattern to not include points outside its boundary because of vignetting. Further, we checked that the spot diagram obtained by using Eq. (6) was within $\lambda/10$, and even $\lambda/20$ in some cases, compared to real finite raytracing.

The values corresponding to the RMS wavefront error, σ_w (in λ units), RMS spot radius σ_s (in λF units), and the P–V (peak-to-valley, in λ units) for each imaging system are listed in Table 2. They have been calculated from the wavefront aberration data in Table 1 and by using Eq. (9) in order to provide quantitative values of their optical correction level.

5. Numerical results

We have plotted the DMTF, $|\tau(\nu)|$, and the GMTF, $|\tau_g(\nu)|$, calculated by using Eqs. (8), and (7), respectively, for each pupil sampling pattern, as well as the difference between them, for each imaging system. We check how good are the sampling patterns

Table 1
Orthonormal Zernike coefficient values (in λ units) obtained by wavefront fitting using optical design software ZEMAX EE.

Zernike coeffs.	Imaging systems					
	On-axis			Off-axis		
	1	2	3	1	2	3
a_1	−1.15	0.19	−1.16	0.71	0.47	−0.29
a_2	0	0	0	0.07	0.22	1.06
a_4	−0.29	0.26	0.11	0.49	0.36	0.06
a_6	0	0	0	0.48	−0.09	−0.19
a_8	0	0	0	0.03	0.04	0
a_{10}	0	0	0	0	−0.01	0.79
a_{11}	0.267	0.04	0.10	0.04	0.05	−0.24
a_{12}	0	0	0	0.11	−0.02	−0.18
a_{16}	0	0	0	0	−0.03	−0.21
a_{22}	−0.11	0	−0.30	−0.02	0	−0.37
a_{37}	0	0	−0.02	0	0	−0.02

Table 2
RMS wavefront error, σ_w (in λ units), RMS spot radius, σ_s (in λF units), and P–V (peak-to-valley, in λ units) values for each imaging system wavefront aberration function, and object point position.

	Imaging systems					
	On-axis			Off-axis		
	1	2	3	1	2	3
σ_w	0.4	0.3	0.7	0.7	0.4	1.4
σ_s	4.7	4.2	8.5	7	4.6	21.5
P–V	1.5	1	1.7	3.2	1.9	7.8

Table 3
Minimum number of pupil sampling points used to obtain a difference between DMTF and GMTF to be about 5% in the low spatial frequency range. Those which fulfilled that criterion are listed in bold type.

Pupil sampling pattern	Imaging systems								
	On-axis			Off-axis					
				Tangential			Sagittal		
	1	2	3	1	2	3	1	2	3
Cartesian (C)	253	**253**	**253**	254	253	**253**	254	**253**	**253**
Polar (P)	217	217	217	217	217	217	217	217	**217**
Hexagonal (H)	217	217	217	217	217	217	217	217	217
Random (R)	193	193	**193**	193	193	193	**193**	193	**193**
Spiral (S)	**77**	**77**	**90**	**77**	**90**	**90**	**77**	**90**	**90**
Bos (B)	136	136	136	136	136	136	136	136	136

when approximating the geometrical approximation of their MTF for on- as well as for off-axis performance, compared to their DMTF.

Table 3 shows the minimum number of sampling points required (in bold type) to get a difference between the DMTF and the GMTF about 5% for each system and for tangential and sagittal direction for off-axis points. An increase of that number does not improve the accuracy. A more detailed discussion for each system is given below.

Figs. 2–4 show how well the GMTF approximates to the DMTF for the double Gauss lens. Regarding any field point, and spatial frequency orientation, we can see that the best approximation is achieved by the spiral pattern, as well as the random one. The worst are by using the Bos, and the non uniform polar patterns. However, it is worth to note that the spiral pattern needs as much as a 40% of those points to provide a good MTF in the geometrical approximation. Further, the number of sampling points in this case is remarkably lower considering those required to obtain a reliable DMTF which is 4096.

The results obtained for the telephoto lens are similar (Figs. 5–7). Further, the on-axis performance extends the spatial frequency range beyond the geometrical approximation to a falloff of the DMTF to around 0.1 (0.4 times the cutoff frequency for on-axis compared to 0.2–0.25 for off-axis). Despite this, the Cartesian pattern (with 253 points), and the spiral one (with 77 and 90 point for on- and off-axis, respectively) still provide a good GMTF compared to the DMTF within a 7% difference up to 0.25 times the cutoff frequency.

Remarkably, as for the double Gauss lens, the spiral pattern requires less points for on- as well as for off-axis points than for any other pattern (as much as a 36% of points). Again, the DMTF needs a set of 4096 points to be accurate.

Finally, those results corresponding to the projection lens (Figs. 8–10) confirm those shown for the other systems. In this case, although the Cartesian, the non uniform polar, and the random patterns approximate well the DMTF (with 4096 points), definitely, the spiral one requires a remarkably less number of sampling points (90 compared to 253, 217 and 193, respectively).

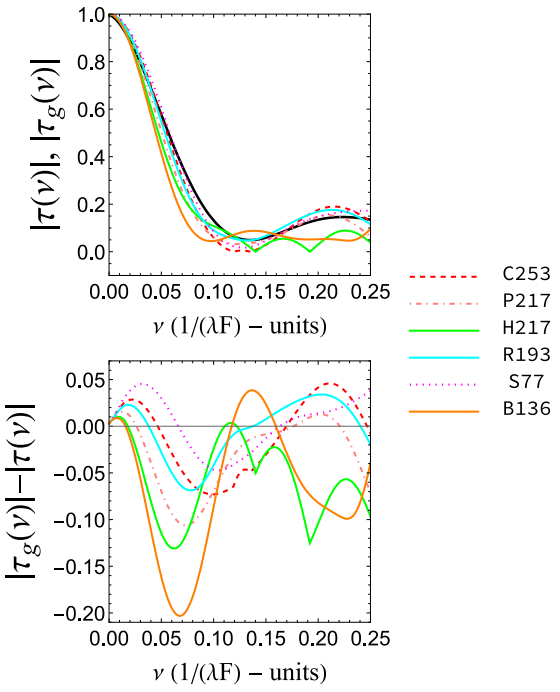

Fig. 2. DMTF (black solid line), and GMTFs obtained by using (7), corresponding to the double Gauss lens, and for on-axis point (upper panel). Difference between DMTF and GMTF, for each pupil sampling pattern (bottom panel). Legend indicates the pattern, and the corresponding number of sampling points utilized.

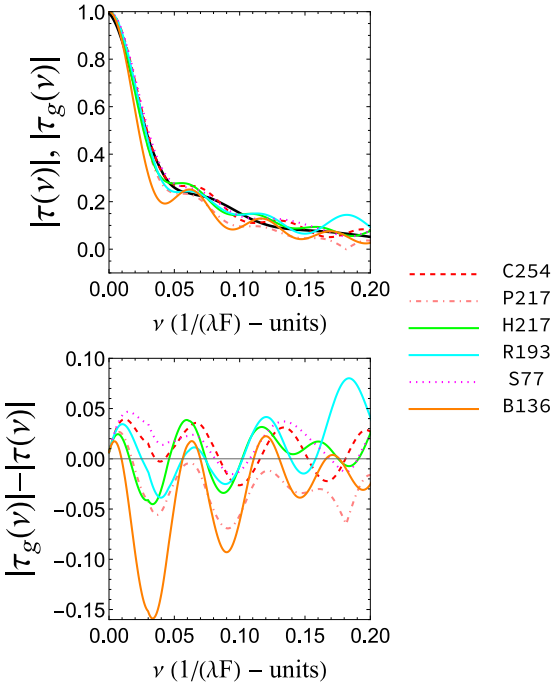

Fig. 3. Same plots as in Fig. 2, but for off-axis point (tangential direction, $\phi = 0$).

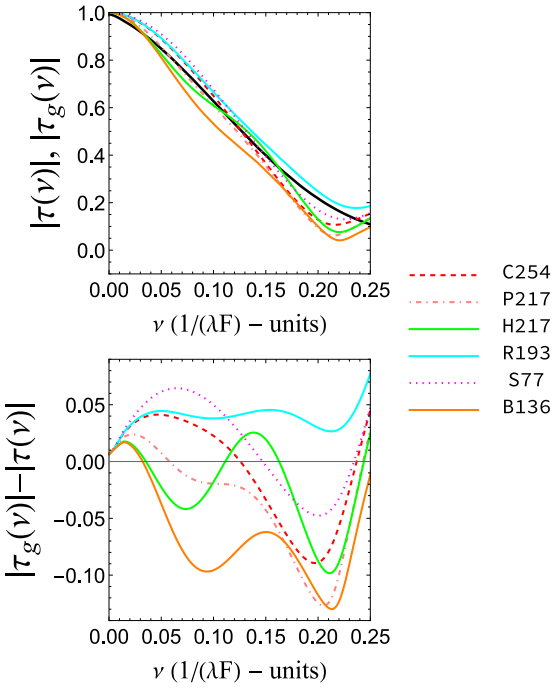

Fig. 4. Same plots as in Fig. 2 for off-axis point (sagittal direction, $\phi = 90$).

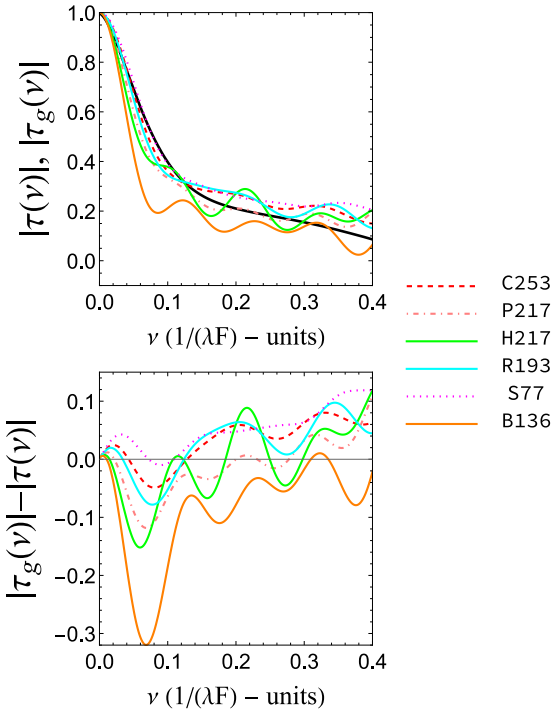

Fig. 5. Same plots as in Fig. 2 but for the telephoto lens, and for on-axis point.

It is worth to make a comment about the sampling points regarding the Bos pattern. As it can be seen in the plot for all the cases studied, the sampling point number was always the same (136). This pattern cannot achieve an accurate geometrical approximation to the DMTF within a threshold of 5%, even increasing the number of sampling points. Therefore, as commented in the Methods Section, that number was not longer increased in seeking to decrease the difference between the DMTF and the GMTF.

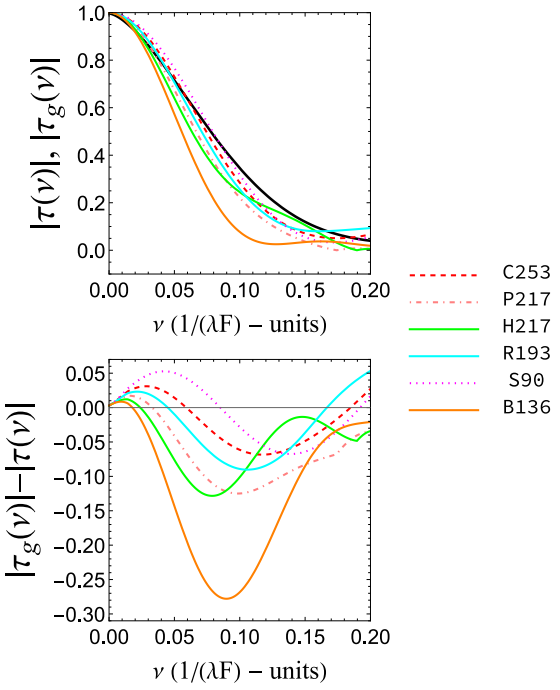

Fig. 6. Same plots as in Fig. 2 but for the telephoto lens, and for off-axis point (tangential direction, $\phi = 0$).

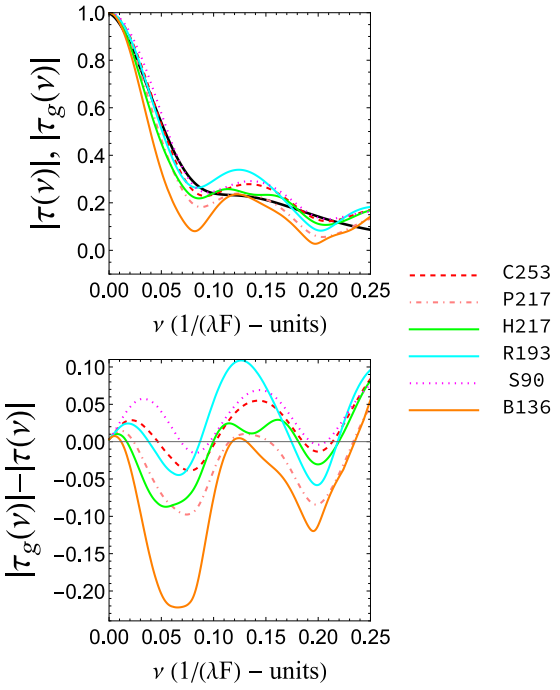

Fig. 7. Same plots as in Fig. 2 but for the telephoto lens, and for off-axis point (sagittal direction, $\phi = 90$).

6. Discussion and conclusions

Designing optical systems relies heavily on raytracing in almost all stages of their design, and this process is quite fast with the help of powerful computers. The data gathered allow to analyze their optical performance by spot diagrams, transverse ray

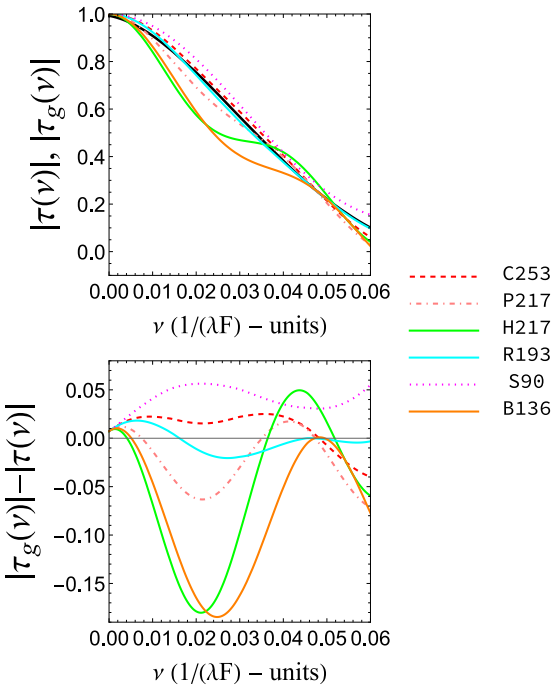

Fig. 8. Same plots as in Fig. 2 but for the projection lens, and for on-axis point.

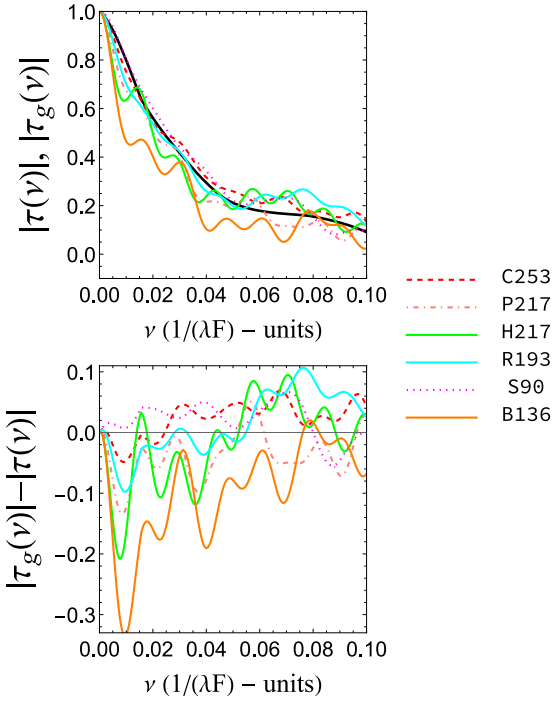

Fig. 9. Same plots as in Fig. 2 but for the projection lens, and for off-axis point (tangential direction, $\phi = 0$).

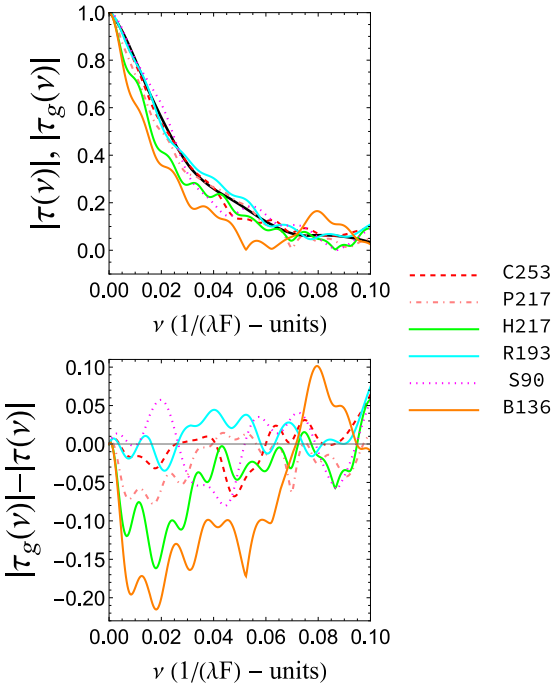

Fig. 10. Same plots as in Fig. 2 but for the projection lens, and for off-axis point (sagittal direction, $\phi = 90$).

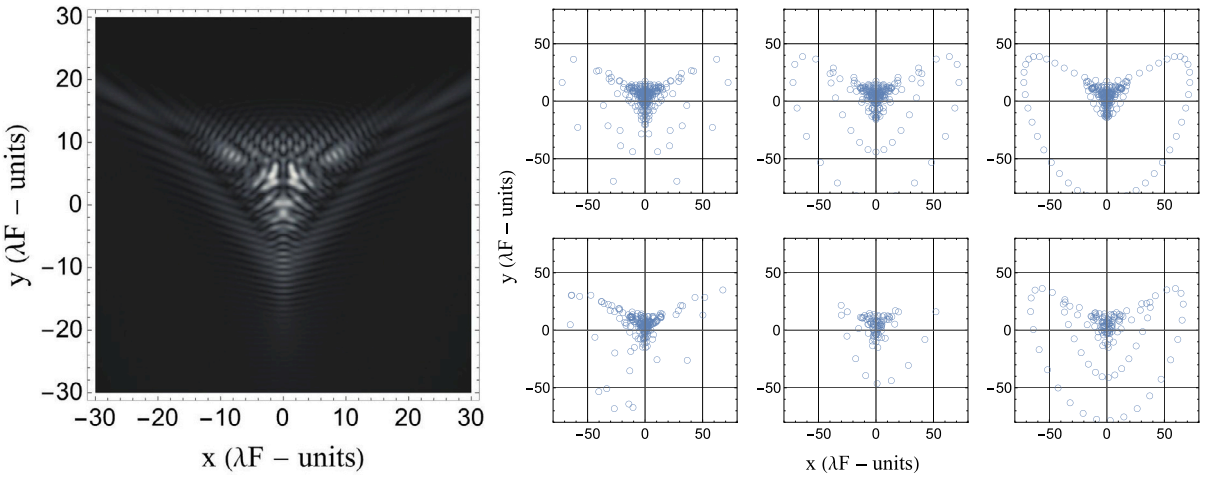

Fig. 11. Left panel: simulated diffraction PSF for off-axis object point at 80° calculated from data in Table 1 for the projection lens. Right panel: corresponding spot diagrams for each sampling pupil pattern (from top left to bottom right: Cartesian, non uniform polar, hexapolar, random, spiral and Bos).

aberrations, optical path difference (OPD) at the exit pupil, and wavefront aberration function. Then, it follows that one can construct the complex pupil function, and compute diffraction based image quality functions, i.e., the PSF, and the OTF.

The point here is that these computations are not reversible. That is, the spot diagram cannot be retrieved from the OTF, which is an important drawback for efficient design optimization. The geometrical approximation may help to overcome this problem by using metrics based on the spot diagram in the optimization process.

Nevertheless, the MTF of the system is essential to know how good is the system when forming images of extended objects at any field point [14,15]. From a practical point of view, the accuracy of the DMTF computation is based on a reliable reconstruction of the wave aberration function from slope or interferometric measurements. There are studies demonstrating that specific sampling patterns are more useful than others in retrieving the wavefront aberration function from slope data. Thus, the spiral as well as the so called Bos pattern have demonstrated to provide a reliable wavefront aberration retrieving in terms of the Zernike polynomials basis, compared to those often used such as the rectangular, hexapolar, random, or polar [27–29].

When the performance of the system is required to be optimal within a range of spatial frequencies low enough with respect to the cutoff frequency, the geometrical approximation to the OTF is valuable [17,23,25]. Although the calculation of the GOTF can be done by using the transverse aberrations (see Eq. (5)), its calculation by means of the FT of the spot diagram data is equally valid (see Eq. (7)) [22,23], and what is more, it does not require to obtain the wavefront aberration function as a previous step in the calculations.

The number of sampling points required to obtain a valuable GMTF is also a key point. The results presented in this study show that we can reduce that number in order that the calculated GMTF will be around, or less than, 5% difference relative to the DMTF. The sampling pattern geometry is even more important.

Eq. (7) shows that all the terms contribute equally, and the higher the values of transverse aberrations (x_i, y_i), the greater the contribution of the wiggly terms in the low frequency range. In Fig. 11, we provide the spot diagrams corresponding to the projection lens for the off-axis object point, as well as the simulated diffraction PSF calculated from the data in Table 1. We can see that the less scattered spot diagram corresponds to that of the spiral sampling. Thus, it should be expected that low spatial frequency terms in Eq. (7) will mainly contribute to the GMTF at low frequencies, and, therefore, the calculated transfer function will be best approximated. The same can be concluded for the other system spot diagrams, and object points.

Hence, the spiral sampling provides, in overall, the best points set to obtain a reliable approximation of the DMTF at low spatial frequencies. In addition, the fact that we do not know the values for the true PSF at each spot diagram point, i.e., the term weight in Eq. (7), is also a drawback for improving the approximation to the DMTF. It is worth highlighting that, overall, the random, the non uniform polar, and the hexapolar pattern provide almost the same number of points compared to the Cartesian one.

However, not only the spiral pattern requires a significant lower sampling points number (about 40 times less compared to those needed to get the DMTF), but this number is also related with the number of Zernike circle polynomials (modes) needed to retrieve the wavefront aberration function accurately, as previous studies have put forward [27–29]. Further, the main computational cost in optimizing complex optical systems is that associated to raytracing. Hence, the spiral pattern would allow computational savings when doing it, since it is related to a decrease in the number of rays traced in the pupil.

In summary, we believe that the spiral sampling pattern can be a very useful tool in the optimization stages of the optical system within the geometrical optics approximation, particularly when the merit function requires the calculation of the MTF in that regime.

Declaration of competing interest

The authors declare that they have no known competing financial interests or personal relationships that could have appeared to influence the work reported in this paper.

Data availability

No data was used for the research described in the article.

Acknowledgments

The authors acknowledge the support to this work given by the Ministerio de Ciencia e Innovación *y* Universidades of Spain (MICIN), grant number PID2019-107058RB-100. Funding for open access charge: Universidad de Granada / CBUA.

References

[1] ZEMAX-EE, ver. 12, Radiant Zemax, LLC., Tucson, AZ, 2012.
[2] OSLO, Lambda Research Corp., Littleton, MA, 2022.
[3] CODE V, Synopsys, Inc., Mountain View, CA, 2022.
[4] SYNOPSYS, ver. 16, Optical Systems Design, LLC, Tucson, AZ, 2022.
[5] R.R. Shannon, The Art and Science of Optical Design, Cambridge University Press, 1997.
[6] H. Gross, Handbook of Optical Systems, Volume 3: Aberration Theory and Correction of Optical Systems, Aberration theory and correction of optical systems, Wiley, 2007.
[7] D. Dilworth, Lens Design, IOP Publishing, 2018.
[8] J. Sasián, Introduction To Lens Design, Cambridge University Press, 2019.
[9] Python Core Team, Python: A dynamic, open source programming language, Python Software Foundation, 2015, (2015). available at https://www.python.org/.
[10] Pyrate: Optical raytracing based on python, 2017, https://salsa.debian.org/mess42/pyrate/.[Online; accessed 1-Sept-2021].
[11] R. Jordens, RayOpt: Python optics and lens design, 2020, https://pypi.org/project/rayopt/. [Online; accessed 1-Sept-2021].
[12] R. Frazier, Pyrayt: The python raytracer, 2017, https://github.com/rfrazier716/PyRayT. [Online; accessed 1-Sept-2021].
[13] J. Herrera, C.A. Guerrero, M.R. Najera, A. Sotelo-Burke, I. Plauchu-Frayn, KrakenOS: Python-based general exact ray tracing library, Opt. Eng. 61 (1) (2022) 1–41.
[14] J.W. Goodman, Introduction To Fourier Optics. 3rd Ed., Roberts and Company Publishers, 2005.
[15] V.N. Mahajan, Optical Imaging and Aberrations II: Wave Diffraction Optics, SPIE Press, 2001.
[16] H. Hopkins, The frequency response of a defocused optical system, Proc. R. Soc. A 231 (1184) (1955) 91–103.
[17] H. Hopkins, Geometrical-optical treatment of frequency response, Proc. Phys. Soc. Sect. B 70 (12) (1957) 1162.
[18] H. Hopkins, The frequency response of optical systems, Proc. Phys. Soc. Sect. B 69 (5) (1956) 562.
[19] N. Bromilow, Geometrical-optical calculation of frequency response for systems with spherical aberration, Proc. Phys. Soc. (1958-1967) 71 (2) (1958) 231.
[20] K. Miyamoto, On a comparison between wave optics and geometrical optics by using Fourier analysis I. General theory, JOSA 48 (1) (1958) 57–63.

[21] K. Miyamoto, Comparison between wave optics and geometrical optics using Fourier analysis II. Astigmatism, coma, spherical aberration, JOSA 48 (8) (1958) 567–575.
[22] K. Miyamoto, Geometrical optical approximation of optical transfer function, Japan. J. Appl. Phys. 3 (S1) (1964) 222.
[23] V.N. Mahajan, J.A. Díaz, Comparison of geometrical and diffraction imaging in the space and frequency domains, Appl. Opt. 55 (12) (2016) 3241–3250.
[24] K. Miyamoto, On a comparison between wave optics and geometrical optics by using Fourier analysis III. Image evaluation by spot diagram, J. Opt. Soc. Amer. 49 (1) (1959) 35–40.
[25] J.A. Díaz, V.N. Mahajan, Geometrical optical transfer function: is it worth calculating? Appl. Opt. 56 (28) (2017) 7998–8004.
[26] V.N. Mahajan, J.A. Díaz, Imaging characteristics of Zernike and annular polynomial aberrations, Appl. Opt. 52 (10) (2013) 2062–2074.
[27] R. Navarro, J. Arines, R. Rivera, Direct and inverse discrete Zernike transform, Opt. Express 17 (26) (2009) 24269–24281.
[28] R. Navarro, J. Arines, R. Rivera, Wavefront sensing with critical sampling, Opt. Lett. 36 (4) (2011) 433–435.
[29] D. Ramos-López, M. Sánchez-Granero, M. Fernández-Martínez, A. Martínez-Finkelshtein, Optimal sampling patterns for Zernike polynomials, Appl. Math. Comput. 274 (2016) 247–257.
[30] L.P. Bos, Near Optimal Location of Points for Lagrange Interpolation in Several Variables (Ph.D. thesis), University of Toronto, 1982.
[31] W.T. Welford, Aberrations of Optical Systems, Routledge, 2017.
[32] V.N. Mahajan, Optical Imaging and Aberrations I: Ray Geometrical Optics, Vol. 45, SPIE Press, 1998.
[33] W. Lukosz, Zur übertragungstheory der inkohärenten optischen abbildung vom standpunket der geometrschen optik, Opt. Acta 5 (1955) 299–305.
[34] Mathematica, ver. 13, Wolfram Research, Inc., Champaign, IL, 2022.
[35] M. Laikin, Lens Design, Fourth, CRC Press, 2018.